

Ultrafast Photo-induced Phase Transition in 2D MoTe₂

Bo Peng,^{1,2,3} Hao Zhang,^{1,*} Weiwen Chen,¹ Zhi-Jun Qiu,⁴ Hezhu Shao,⁵
Heyuan Zhu,¹ Bartomeu Monserrat,³ Desheng Fu,^{6,†} and Hongming Weng^{2,‡}

¹Key Laboratory of Micro and Nano Photonic Structures (MOE),
Department of Optical Science and Engineering, Fudan University, Shanghai 200433, China

²Beijing National Laboratory for Condensed Matter Physics,
and Institute of Physics, Chinese Academy of Sciences, Beijing 100190, China

³TCM Group, Cavendish Laboratory, University of Cambridge,
J. J. Thomson Avenue, Cambridge CB3 0HE, United Kingdom

⁴State Key Laboratory of ASIC & System, School of Information Science and Technology, Fudan University, Shanghai 200433, China

⁵Ningbo Institute of Materials Technology and Engineering, Chinese Academy of Sciences, Ningbo 315201, China

⁶Department of Electronics & Materials Sciences, Faculty of Engineering,
& Department of Optoelectronics and Nanostructure Science,

Graduate School of Science and Technology, Shizuoka University, Hamamatsu, 432-8561, Japan

Photo-induced phase transition (PIPT) provides an ultrafast, energy-efficient way for precisely manipulating the topological properties in transition-metal ditellurides, and can be used to stabilize a topological phase in an otherwise semiconducting phase. Using two-dimensional (2D) monolayer MoTe₂ as an example, we demonstrate that the PIPT from semiconducting 2H to topological 1T' phase is induced purely by electronic excitations from first-principles calculations. Such photo-induced electronic excitation changes electron density, modifying the chemical bonding and hence softening the lattice vibrational modes. These pronounced softenings lead to structural symmetry breaking within sub-picosecond, which is far shorter than the timescale of thermally driven phase transition. The transition can be triggered by photons with energy over 2.34 eV, corresponding to a critical excited carrier density of $10.1 \times 10^{14} \text{ cm}^{-2}$, which enables controllable phase transformation by varying laser wavelength. Our results show an ultrafast and controllable phase transition mechanism for topological switching applications of 2D systems, paving the way for future 2D material-based science and technology.

The *photo-induced phase transitions* (PIPT), which is resulted from cooperative electron-lattice interactions through changing the electronic states and local nonequilibrium states of the solid transiently by photo-excitations¹, is completely different from thermal or pressure-induced phase transitions caused by spontaneous symmetry breaking. PIPT not only allows us to access the hidden multi-stable states in the solid to explore the local non-equilibrium dynamics and the anomalous properties absent in the ground-state phase, but also enables precisely controllable phase transition towards target structures with desired physical properties at high speeds. Thus, the initial discovery of PIPT in organic charge transfer crystal has triggered great interests in broad fields. Compared with the vast materials with the thermal-dynamics phase transition, solid with PIPT is still very limited and many of the investigations are focused on the bulk crystals possessing one-dimensional (1-D) correlated electron chains that PIPT may be easily triggered due to the inherent instabilities of electron-electron and/or electron-lattice interactions in the system¹.

As an emerging platform for PIPT, two-dimensional (2D) layered transition-metal ditellurides exhibit polymorphisms with distinct physical properties²⁻⁴. Recent experimental evidence for PIPT in MoTe₂ and WTe₂ has demonstrated that structural phase transitions often involve abrupt changes in the electronic structures and the emergence of novel topological states⁵⁻⁷. For instance, in few-layer MoTe₂, an irreversible transition from semiconducting hexagonal 2H phase to topological distorted octahedral 1T' phase occurs under laser irradiations, which can be used to fabricate an ohmic heterophase homojunction with accurate control of micron-patterning in a desired area⁵. Such structural distortion results in an intrinsic

band inversion between Te *p* and Mo *d* bands^{8,9}, enabling ultrafast manipulation of the topological properties for topological switch devices. The topological phases also display gate-tunable superconductivity, providing a new platform to realize Majorana bound modes^{10,11}.

However, the exact nature for such phase transition remains unclear. Triggered by external stimulation of light, the system undergoes several stages with changes in both internal and external conditions such as temperature, strain, electronic excitation, chemical state and lattice vibrational modes. The transitions may depend on several factors or a combination of them^{5,12}. It has been supposed that Te vacancies created by irradiation trigger the local phase transition^{5,13,14}. Besides, previous theoretical and experimental studies have also argued that accumulated heating effect is a main driving force for phase transition^{13,15}. Moreover, strain-induced phase transition has been observed in monolayer MoTe₂^{16,17}, thus laser-induced thermal strain may also contribute to the observed phase transition. Another explanation is that the electronic excitation plays a critical role in the phase transition^{18,19}, but the transition mechanism is still in debate.

Here, we demonstrate that the phase transition of monolayer MoTe₂ can be triggered by electronic excitation alone. Photoexcitation weakens the chemical bonds by real-space electron transfer, resulting in softening of lattice vibrations that leads to a spontaneous structural distortion with new equilibrium positions for atoms. The phase transition can take place within one picosecond before the thermalized electrons transfer their energy to the lattice. Finally, we rule out thermally-driven and strain-induced phase transition under laser irradiations by studying thermodynamic stability of

2H and 1T' MoTe₂ monolayers. Our findings not only reveal the origin of PIPT in 2D transition-metal ditellurides, but also provide new insight in the observed dynamic transitions in their 3D counterparts that remains elusive^{6,20,21}.

All calculations are performed based on density functional theory (DFT) using the Vienna *ab-initio* simulation package (VASP)²² (for details, see Computational Details in JOINT SUBMISSION). The crystal structures of 2H and 1T' MoTe₂ monolayers are described in JOINT SUBMISSION. We use a nonprimitive rectangular unit cell for the 2H phase in comparison with the 1T' phase. The semiconducting 2H phase is characterized by a hexagonal *P-6m2* unit cell with a trigonal prismatic arrangement of Te ligands around the central Mo atom. The 1T' phase possesses an orthorhombic *P2₁/m* structure with a distorted octahedral coordination of the Mo atoms, in which the Te atoms in the two opposite planes stagger, resulting in a semi-metallic electronic structure with complex topological states²³.

Photo-induced change in electronic state. Upon optical irradiation, electrons are excited in the 2H lattice before the structural reorganizations, inducing ultra-rapid bond dissociation²⁴. We firstly examine how the photoexcitation changes the electronic state in the system. Fig. 1 shows the electron localization function of 2H MoTe₂ under 1.58 eV (785 nm), 1.96 eV (633 nm), 2.34 eV (532 nm), 2.42 eV (514 nm), and 2.63 eV (473 nm) laser excitation energies by moving valence electrons to the conduction band to mimic optical excitation.

As shown in Fig. 1(b), the electrons in the Mo layer are gathered between top and bottom Te atoms under an optical excitation of 2.34 eV, increasing the degeneracy of electronic states. According to the Jahn-Teller theorem, degenerate electronic states are unstable²⁵. Such degeneracy can be removed by distortions. This is clarified by the change of electron distribution in the Mo layer in Fig. 1(c). At 1.58 eV, the electron distribution around Mo atoms changes from isolated triangles to connected hexagons. As the excitation energy increases to 1.96 eV, the triangles appear once again, but with a reversed orientation. Such change in electronic states tends to induce irreversible displacements of the E'' and E' modes [Fig. 2(b)]. With further increasing excitation energies, the change becomes more remarkable, leading to phase instability.

Photo-induced lattice mode softening. Upon optical excitation, the chemical bonds in MoTe₂ become unstable, and structural distortions hence arise. We examine the atomic displacements in excited 2H phase. With *D_{3h}* point group, the irreducible representations of the vibrational modes in 2H phase can be expressed as²⁶

$$\Gamma_{2H} = E'' + A'_1 + E' + A''_2. \quad (1)$$

The calculated phonon dispersion is present in Fig. 2(a) with the optical phonon modes at the Γ point marked. The calculated lattice mode frequencies [Fig. 2(b)] are consistent with previous reports^{27,28}.

We then focus on three modes (E'', E' and A''₂) corresponding to the three primary lattice distortions along the pathway from the 2H to 1T' phase (for details, see Crystal Structures in JOINT SUBMISSION). We calculate the potential energy

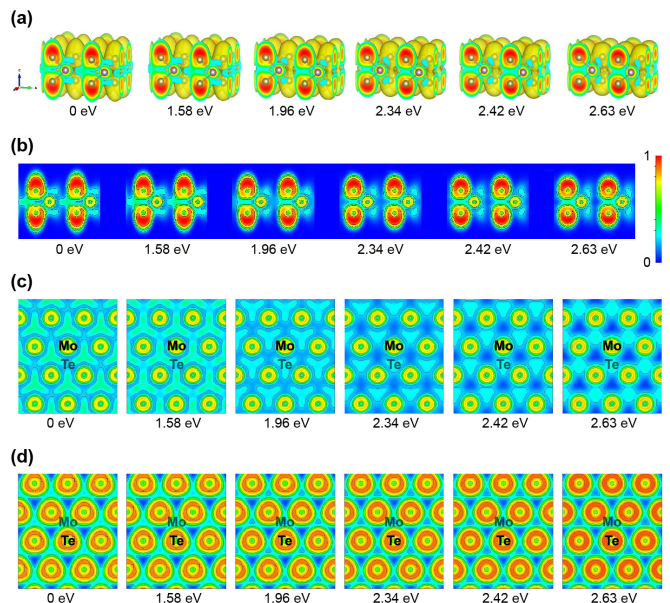


FIG. 1. (a) 3D, (b) side view, top view of (c) Mo layer and (d) Te layer of electron localization function of monolayer MoTe₂ at different excitation energies before the lattice is rearranged. Increasing electron localization from 0 to 1 is plotted with colours from navy to red. The isosurfaces for electron localization function in (a) is 0.2.

landscape as a function of displacement amplitude of these vibrations under different photoexcitation energies to investigate the phase instability. The results are summarized in Fig. 2(c)-(e), with the energy of the excited 1T' phase set as zero for comparing the relative stability between the 2H and 1T' phases. In the ground state, the 2H phase has lower energy than the 1T' phase. However, as the system is optically excited, the 2H phase becomes energetically less favorable than the 1T' phase due to population inversion¹⁸, which is consistent with previous results¹⁹.

Under optical excitation, these three atomic displacements lead to structural phase transitions along the pathway from the 2H to 1T' phase. For the E'' mode (corresponding to the opposite in-plane motion of top and bottom Te layers), the Te atoms vibrate harmonically around their equilibrium positions before photoexcitation. The potential energy surface becomes flattened gradually with increasing excitation energy, and a double-well potential is formed at 2.63 eV. Thus the Te atoms have two energetically equivalent sites, and a distorted octahedral structure can be formed in excited state (purple circle 1 in Fig. 2). A similar situation occurs for the A''₂ mode (an out-of-plane displacement of Mo atoms and an opposite-direction displacement of Te atoms). With an excitation higher than 2.34 eV, the Mo atoms can bounce up or down in the two minima, while the Te atoms move in opposite directions, leading to an out-of-plane atomic movement. One possible intermediate structure is an out-of-plane distorted variant of 2H MoTe₂ (purple circle 2 in Fig. 2). The evolution of the E' mode under irradiation is slightly different. This mode composed of in-plane displacements with the one Mo layer and the two Te layers moving opposite to each other. Increasing optical

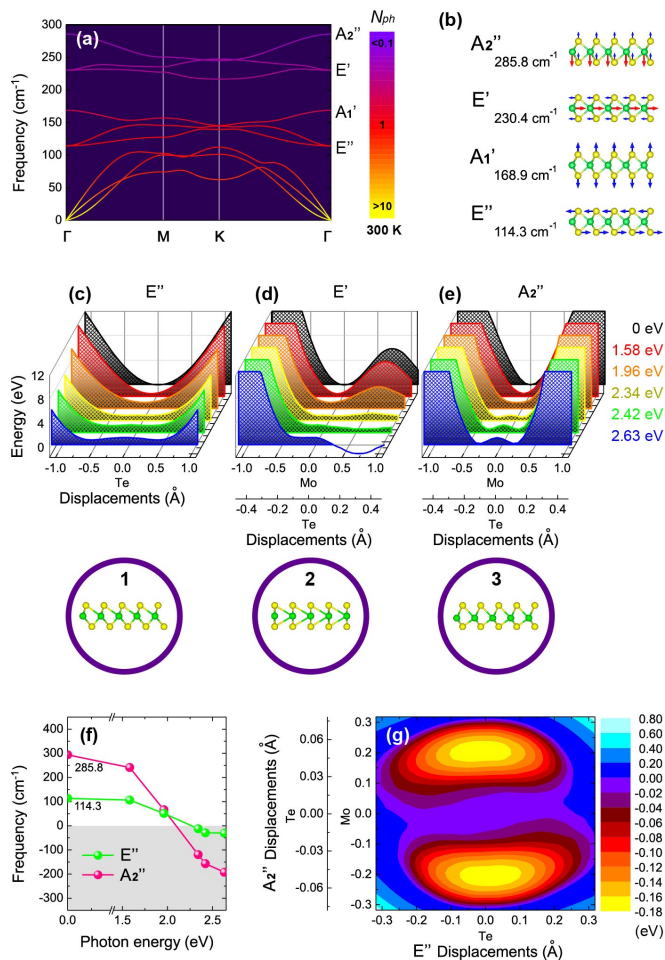


FIG. 2. (a) Phonon dispersion and (b) vibrational modes for optical phonons at the Γ point. The phonon occupation number is determined from the Bose-Einstein distribution function at 300 K. At different excitation energies, the potential energy surface along the eigenvectors of (c) E'' mode, (d) E' mode, and (e) A_2'' mode at different excitation energies. The energies of the excited $1T'$ crystal at different excitation energies are set as zero. The purple circles denoted by 1, 2, 3 correspond to a finite displacement along the eigenvectors that leads to a structure with a minimum energy for the excited crystal. These intermediate crystal structures, as shown in the enlarged circles in (c), (d), and (e), lead to the three primary lattice distortions along the pathway from the $2H$ to $1T'$ phase. (f) Energy surface in the plane spanned by the two soft modes. Each contour line represents an energy increase of 0.02 eV. (g) Phonon frequency of the E'' and A_2'' modes as a function of laser excitation energy.

excitation energy lowers the energy barrier for positive displacements along the eigenvector of the E' mode. This barrier is flattened at excitation energies over 2.34 eV, and becomes a deep well at 2.63 eV. In the intermediate structure corresponding to this deep well (purple circle 3 in Fig. 2), top Te, center Mo, and bottom Te atoms are aligned and the Mo-Te bonds are shortened. After cessation of the excitation, the energy barrier reappears. As a result, Mo and Te atoms in that intermediate structure bounce back and forth randomly, resulting in distorted in-plane atomic positions, which yields a better

packing of the Te-Mo-Te sub-lattice along the phase transition pathway from $2H$ to $1T'$ MoTe_2 , corresponding to the twisted octahedral coordination around Mo atoms.

To describe the phonon softening quantitatively, we calculate the phonon frequency of the E'' and A_2'' modes as a function of photoexcitation energy by fitting the second-order (and fourth-order) term in energy surface potential²⁹. As shown in Fig. 2(f), the phonon frequencies start to soften at 1.58 eV. The phonon frequency of E'' (A_2'') drop to zero at excitation energies around 2.3 (2.1) eV. Thus the PIPT occurs at a minimum excitation energy of 2.34 eV. Our findings on photo-induced lattice mode softening at 2.34 eV, marked by clear changes in both Raman and infrared spectra, can be easily verified experimentally by ultrafast coherent phonon spectroscopy²⁰ or second harmonic generation³⁰.

Such spontaneous lattice distortions can be described by the energy surface in the subspace spanned by the soft modes³¹. Fig. 2(g) shows the energy surface mapped on the plane spanned by the two soft modes E'' and A_2'' at the photoexcitation energy of 2.34 eV. The two equivalent minima correspond to the possible distortions for finite displacements along the eigenvector of the A_2'' mode. These atomic rearrangements may decay to the $1T'$ phase as they are intermediate structures from $2H$ to $1T'$. Previous experiments have demonstrated that, for laser-irradiated mixed $2H + 1T'$ phase, the $2H$ phase disappears completely after annealing, leaving a pure $1T'$ crystal; whereas for pure $2H$ MoTe_2 , no significant change occurs after annealing¹⁵. Thus electronic excitation is the main driving force to induce spontaneous lattice distortions, while heating effect accelerates the phase transition by thermal displacement.

In addition, the phase transition is irreversible because the $1T'$ phase formed in the electronically excited state is metastable. To return to the ground-state $2H$ phase, the system has to overcome a potential barrier^{18,19}. Therefore, the subsequent stabilization of the $1T'$ phase can be achieved after cessation of the excitation. It has been observed that the laser-induced $1T'$ MoTe_2 is stable for more than one week in ambient conditions without any protection¹⁵.

Excited carrier concentrations. The larger the excitation energies, the more electrons are excited. Table I shows the excited carrier concentrations under different excitation energies. The critical excited carrier density to induce PIPT is $10.1 \times 10^{14} \text{ cm}^{-2}$, corresponding to the excitation energy of 2.34 eV. A laser with an energy higher than 2.34 eV can readily generate excitations in excess of 8.5%. We also estimate the

TABLE I. Excited carrier concentration n and the maximum amount of excitation N by a laser pulse with a fluence of 100 mJ/cm^2 , as well as their corresponding excitation percentage in the total number of valence electrons N_{tot} , at different laser excitation energies.

Energy (eV)	1.58	1.96	2.34	2.42	2.63
$n (\times 10^{14} \text{ cm}^{-2})$	0.9	3.4	10.1	11.8	13.2
$n/N_{\text{tot}} (\%)$	0.8	2.9	8.5	9.9	11.1
$N (\times 10^{14} \text{ cm}^{-2})$	7.2	12.2	16.0	17.2	17.6
$N/N_{\text{tot}} (\%)$	6.0	10.2	13.5	14.5	14.8

maximum amount of electron-hole pairs generated by a femtosecond laser with a fluence of 100 mJ/cm^2 ^{232,33}. As shown in Table I, up to 14.8% excitation is possible. Thus the excited carrier concentrations in our calculations are reasonable estimations. As PIPT can take place for excitation over 8.5% (2.34 eV), a laser pulse with a fluence of 100 mJ/cm^2 is sufficient, and the minimum fluence for phase transition is calculated to be 63 mJ/cm^2 . This is consistent with the experimental fact that with insufficient laser power, the phase transformation cannot take place completely even for long irradiation time^{5,15}.

The hot carrier population is related to the density of states (DOS)³⁴. The electronic structures [Fig. 3(a)] agree well with previous results^{35,36} (for details on the band gap and spin splitting, see Electronic Structure and Optical Properties in JOINT SUBMISSION). As shown in Fig. 3(c), the saddle points in the band structure give large DOS. The electronic excitation energies of 2.52 eV, 2.74 eV, and 2.96 eV correspond to the optical transitions between the peaks in the DOS. In 2D materials, reduced electronic screening typically leads to strong excitonic effect³⁷. By including electronhole interactions, the calculated imaginary part of dielectric function ϵ_2 shows a non-zero value above the photon energy of 1.0 eV [Fig. 3(d)], which agrees well with the optical absorption measurement³⁸. Because of the electron-hole attraction, the optical transition energies [marked by arrows in Fig. 3(c)] are reduced to 2.22 eV, 2.45 eV, and 2.68 eV. With laser energies larger than 2.22 eV, the concentrations of excited carriers become higher, corresponding to strong optical excitation. Moreover, the electronic excitation energies of 2.45 eV and 2.68 eV match well with the laser energies of 2.42 eV and 2.63 eV.

Timescale of the phase transition. The timescale after laser excitation is divided into four regimes:

In the first stage, the temperature of the electronic systems increases rapidly within 120 fs, while the lattice remains cold. In photoexcited MoTe₂, carrier-carrier scattering is responsible for redistributing carrier energy, resulting in a thermalized distribution function of carriers³⁹. The carrier relaxation time can be calculated from the quasiparticle self-energy^{37,40}. As shown in Fig. 3(b), electrons and holes thermalize themselves in 20 fs. In addition, exciton-exciton interaction leads to a thermalized, hot exciton distribution. The exciton lifetime can be calculated from the electron-hole amplitude and the quasiparticle self-energy^{37,41}. As shown in Fig. 3(f), the electron-hole pairs achieve a common temperature in 120 fs. In this stage, all the carriers and excitons are in equilibrium before interacting with phonons.

In the second stage, the symmetry breaking displacements in 2H MoTe₂ take place within 292 fs. As the laser pulse creates electronic excitations, the new potential energy surfaces in Fig. 2(c)-(e) are formed immediately. The photo-induced lattice distortions, as a result of phonon softening, occur within a timescale of lattice vibrations. This can be estimated by the lattice vibration period from 117 fs (A_2'' mode) to 292 fs (E'' mode). Such an estimation agrees well with previous molecular dynamics simulations¹⁸ and pump-probe spectroscopy²⁰. Because the timescale for carrier-phonon interaction is 1-100 ps³⁹, the structural distortion can take place

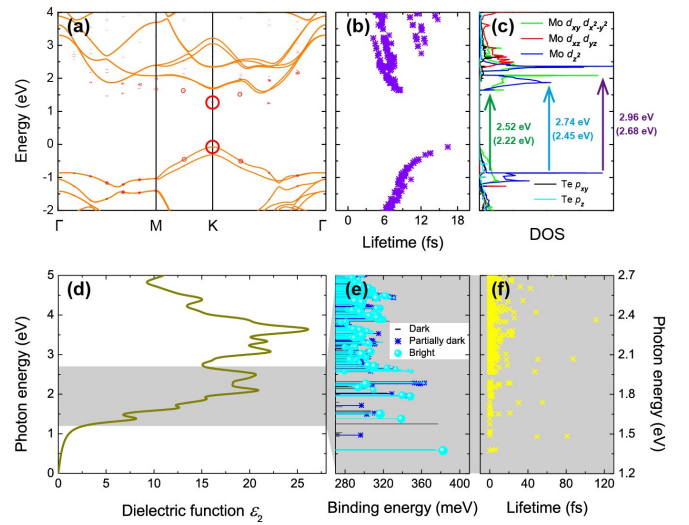


FIG. 3. (a) Electronic structures, (b) quasiparticle relaxation time, and (c) DOS of monolayer MoTe₂. The red circles in (a) denote the first exciton. The radius of circles represents the electronhole coupling coefficient of excitonic wave functions. The larger the radius, the more an electron-hole pair contributes to the exciton eigenstate. The arrows in (c) indicate optical transitions with different electronic excitation energies. The parentheses in (c) show the exciton excitation energies. (d) Imaginary part of dielectric function ϵ_2 , (e) dark, partially dark, and bright excitons with different binding energies, and (f) exciton lifetime for monolayer MoTe₂. The radius of circles in (e) represents the oscillator strength for bright excitons.

before the electrons transfer their energy to the lattice.

In the third stage, the hot electrons, holes and excitons are cooled by transferring energy to the lattice, converting electronic photoexcitation energy to heat in hundreds of picoseconds through interaction with various phonons. It should be noticed that a transition from the 2H phase to a distorted phase can be triggered by purely electronic excitation when most energy remains within the excited electronic system. Some argue that, after the excited electrons are instantly relaxed to lattice heat through electron-phonon coupling, atomic reorganization toward the 1T' phase may occur as a result of local heat¹³ or thermal strain^{16,17}. We demonstrate that these thermal effects alone cannot trigger phase transition: Only at temperatures higher than 930 K, 1T' MoTe₂ becomes thermodynamically more stable than the 2H phase (for details, see Thermal Effects in JOINT SUBMISSION). This is consistent with the experimental evidence that the pure 1T' phase appears at 930 K under Te deficiency²³. However, the temperature to facilitate phase transition, 930 K, is much higher than the laser-induced temperature of 670 K⁵. Even after taking thermal strain into consideration, the phase transition temperature of 770 K is still higher than the laser-induced temperature (for details, see Thermal Effects in JOINT SUBMISSION). Therefore the laser-induced thermal effect on phase transition is probably overestimated in previous results^{5,13}.

Compared to thermal-induced or strain-driven structural phase transformation, optically induced electronic excitation offers high precision control of phase transition. The phase

patterning can be achieved controllably with sub-micron precision⁵. In addition, electronic excitation enables faster phase transformation on a timescale of sub picosecond, much faster than thermally induced phase transition. Moreover, if the heat generated during the electronic excitation can be removed by cooling, thermal effects such as anharmonicity and melting can be suppressed.

In summary, we demonstrate that purely electronic excitation can trigger sub-picosecond phase transition in 2H MoTe₂ monolayer. Increasing optical excitation energy destabilizes the 2H crystal structure, flattening and softening the potential energy surfaces for phonon vibrations. Lattice distortions by these vibrational modes lead to the formation of the intermediate crystal structures in the pathway between the 2H and 1T' phases. In addition, the 1T' phase becomes more energetically favourable in the electronically excited state, and the system can end up in such metastable state to reach the lower energy through spontaneous symmetry breaking. Such phase transformation is wavelength-dependent because the density of excited charge carriers increases monotonically with increasing

optical excitation energy. Our calculations on hot carrier and exciton dynamics show that the phase transition can take place even when the lattice is still cold, while thermal effects alone cannot induce the phase transition. Therefore, fast and precise control of selective phase transition is achievable and feasible by changing the laser wavelength, offering new opportunities for optical modulators, topological switching devices and neuromorphic computing.

The authors gratefully acknowledge helpful discussions with Ms. Fangyuan Gu at Imperial College London and Prof. Xian-Bin Li at Jilin University. This work is supported by the National Natural Science Foundation of China under Grants No. 11374063, 11674369, 11404348 and 61774042, the National Key Research and Development Program of China (No. 2016YFA0300600 and 2018YFA0305700), the ‘‘Strategic Priority Research Program (B)’’ of the Chinese Academy of Sciences (Grant No. XDB07020100), and MEXT KAKENHI Grant Number JP17K05031, and Shanghai Municipal Natural Science Foundation (17ZR1446500).

-
- * zhangh@fudan.edu.cn
† fu.tokusho@shizuoka.ac.jp
‡ hmweng@iphy.ac.cn
- ¹ K. Nasu, ed., *Photoinduced phase transitions* (World Scientific, 2004).
 - ² Y. Wang, J. Xiao, H. Zhu, Y. Li, Y. Alsaïd, K. Y. Fong, Y. Zhou, S. Wang, W. Shi, Y. Wang, A. Zettl, E. J. Reed, and X. Zhang, *Nature* **550**, 487 (2017).
 - ³ Z. Fei, W. Zhao, T. A. Palomaki, B. Sun, M. K. Miller, Z. Zhao, J. Yan, X. Xu, and D. H. Cobden, *Nature* **560**, 336 (2018).
 - ⁴ F. Zhang, H. Zhang, S. Krylyuk, C. A. Milligan, Y. Zhu, D. Y. Zemlyanov, L. A. Bendersky, B. P. Burton, A. V. Davydov, and J. Appenzeller, *Nature Materials* **18**, 55 (2019).
 - ⁵ S. Cho, S. Kim, J. H. Kim, J. Zhao, J. Seok, D. H. Keum, J. Baik, D.-H. Choe, K. J. Chang, K. Suenaga, S. W. Kim, Y. H. Lee, and H. Yang, *Science* **349**, 625 (2015).
 - ⁶ E. J. Sie, C. M. Nyby, C. D. Pemmaraju, S. J. Park, X. Shen, J. Yang, M. C. Hoffmann, B. K. Ofori-Okai, R. Li, A. H. Reid, S. Weathersby, E. Mannebach, N. Finney, D. Rhodes, D. Chenet, A. Antony, L. Balicas, J. Hone, T. P. Devereaux, T. F. Heinz, X. Wang, and A. M. Lindenberg, *Nature* **565**, 61 (2019).
 - ⁷ H. Yang, S. W. Kim, M. Chhowalla, and Y. H. Lee, *Nature Physics* **13**, 931 (2017).
 - ⁸ X. Qian, J. Liu, L. Fu, and J. Li, *Science* **346**, 1344 (2014).
 - ⁹ D.-H. Choe, H.-J. Sung, and K. J. Chang, *Phys. Rev. B* **93**, 125109 (2016).
 - ¹⁰ E. Sajadi, T. Palomaki, Z. Fei, W. Zhao, P. Bement, C. Olsen, S. Luescher, X. Xu, J. A. Folk, and D. H. Cobden, *Science* **362**, 922 (2018).
 - ¹¹ V. Fatemi, S. Wu, Y. Cao, L. Bretheau, Q. D. Gibson, K. Watanabe, T. Taniguchi, R. J. Cava, and P. Jarillo-Herrero, *Science* **362**, 926 (2018).
 - ¹² S. Kretschmer, H.-P. Komsa, P. Boggild, and A. V. Krasheninnikov, *J. Phys. Chem. Lett.* **8**, 3061 (2017).
 - ¹³ Z. Wang, X. Li, G. Zhang, Y. Luo, and J. Jiang, *ACS Appl. Mater. Interfaces* **9**, 23309 (2017).
 - ¹⁴ A. Yoshimura, M. Lamparski, N. Kharche, and V. Meunier, *Nanoscale* **10**, 2388 (2018).
 - ¹⁵ Y. Tan, F. Luo, M. Zhu, X. Xu, Y. Ye, B. Li, G. Wang, W. Luo, X. Zheng, N. Wu, Y. Yu, S. Qin, and X.-A. Zhang, *Nanoscale* **10**, 19964 (2018).
 - ¹⁶ K.-A. N. Duerloo, Y. Li, and E. J. Reed, *Nature Communications* **5**, 4214 (2014).
 - ¹⁷ S. Song, D. H. Keum, S. Cho, D. Perello, Y. Kim, and Y. H. Lee, *Nano Lett.* **16**, 188 (2016).
 - ¹⁸ A. V. Kolobov, P. Fons, and J. Tominaga, *Phys. Rev. B* **94**, 094114 (2016).
 - ¹⁹ A. Krishnamoorthy, L. Bassman, R. K. Kalia, A. Nakano, F. Shimajo, and P. Vashishta, *Nanoscale* **10**, 2742 (2018).
 - ²⁰ M. Zhang, Z. Wang, Y. Li, L. Shi, D. Wu, T. Lin, S. Zhang, Y. Liu, C. Wang, Q. Liu, J. Wang, T. Dong, and N. L. Wang, arXiv: **1806**, 09075 (2018).
 - ²¹ H.-J. Kim, S.-H. Kang, I. Hamada, and Y.-W. Son, *Phys. Rev. B* **95**, 180101 (2017).
 - ²² G. Kresse and J. Furthmüller, *Phys. Rev. B* **54**, 11169 (1996).
 - ²³ D. H. Keum, S. Cho, J. H. Kim, D.-H. Choe, H.-J. Sung, M. Kan, H. Kang, J.-Y. Hwang, S. W. Kim, H. Yang, K. J. Chang, and Y. H. Lee, *Nature Physics* **11**, 482 (2015).
 - ²⁴ N.-K. Chen, D. Han, X.-B. Li, F. Liu, J. Bang, X.-P. Wang, Q.-D. Chen, H.-Y. Wang, S. Zhang, and H.-B. Sun, *Phys. Chem. Chem. Phys.* **19**, 24735 (2017).
 - ²⁵ H. A. Jahn and E. Teller, *Proceedings of the Royal Society of London. Series A, Mathematical and Physical Sciences* **161**, 220 (1937).
 - ²⁶ M. Yamamoto, S. T. Wang, M. Ni, Y.-F. Lin, S.-L. Li, S. Aikawa, W.-B. Jian, K. Ueno, K. Wakabayashi, and K. Tsukagoshi, *ACS Nano* **8**, 3895 (2014).
 - ²⁷ M. Kan, H. G. Nam, Y. H. Lee, and Q. Sun, *Phys. Chem. Chem. Phys.* **17**, 14866 (2015).
 - ²⁸ H. Guo, T. Yang, M. Yamamoto, L. Zhou, R. Ishikawa, K. Ueno, K. Tsukagoshi, Z. Zhang, M. S. Dresselhaus, and R. Saito, *Phys. Rev. B* **91**, 205415 (2015).
 - ²⁹ B. Monserrat, *Journal of Physics: Condensed Matter* **30**, 083001 (2018).
 - ³⁰ Y. Song, R. Tian, J. Yang, R. Yin, J. Zhao, and X. Gan, *Advanced Optical Materials* **6**, 1701334 (2018).

- ³¹ J. C. A. Prentice, B. Monserrat, and R. J. Needs, *Phys. Rev. B* **95**, 014108 (2017).
- ³² K. Sokolowski-Tinten, J. Bialkowski, and D. von der Linde, *Phys. Rev. B* **51**, 14186 (1995).
- ³³ X.-B. Li, X. Q. Liu, X. Liu, D. Han, Z. Zhang, X. D. Han, H.-B. Sun, and S. B. Zhang, *Phys. Rev. Lett.* **107**, 015501 (2011).
- ³⁴ M. Bernardi, D. Vigil-Fowler, J. Lischner, J. B. Neaton, and S. G. Louie, *Phys. Rev. Lett.* **112**, 257402 (2014).
- ³⁵ A. Ramasubramaniam, *Phys. Rev. B* **86**, 115409 (2012).
- ³⁶ C. Ruppert, O. B. Aslan, and T. F. Heinz, *Nano Lett.* **14**, 6231 (2014).
- ³⁷ B. Peng, H. Zhang, H. Shao, K. Xu, G. Ni, L. Wu, J. Li, H. Lu, Q. Jin, and H. Zhu, *ACS Photonics* **5**, 4081 (2018).
- ³⁸ I. G. Lezama, A. Arora, A. Ubaldini, C. Barreateau, E. Giannini, M. Potemski, and A. F. Morpurgo, *Nano Lett.* **15**, 2336 (2015).
- ³⁹ J. Shah, *Ultrafast spectroscopy of semiconductors and semiconductor nanostructures* (Springer Science & Business Media, 2013).
- ⁴⁰ T. Kotani and M. van Schilfgaarde, *Phys. Rev. B* **81**, 125201 (2010).
- ⁴¹ K. F. Mak, F. H. da Jornada, K. He, J. Deslippe, N. Petrone, J. Hone, J. Shan, S. G. Louie, and T. F. Heinz, *Phys. Rev. Lett.* **112**, 207401 (2014).